Research article **Open Access**

Tong Wang*, Tim J. Puchtler, Saroj K. Patra*, Tongtong Zhu, Muhammad Ali, Tom J. Badcock, Tao Ding, Rachel A. Oliver, Stefan Schulz and Robert A. Taylor

Direct generation of linearly polarized single photons with a deterministic axis in quantum dots

DOI 10.1515/nanoph-2017-0027
Received February 20, 2017; revised April 20, 2017; accepted April 24, 2017

Abstract: We report the direct generation of linearly polarized single photons with a deterministic polarization axis in self-assembled quantum dots (QDs), achieved by the use of non-polar InGaN without complex device geometry engineering. Here, we present a comprehensive investigation of the polarization properties of these QDs and their origin with statistically significant experimental data and rigorous **k·p** modeling. The experimental study of 180 individual QDs allows us to compute an average polarization degree of 0.90, with a standard deviation of only 0.08. When coupled with theoretical insights, we show that these QDs are highly insensitive to size differences, shape anisotropies, and material content variations. Furthermore, 91% of the studied QDs exhibit a polarization axis along the crystal [1–100] axis, with the other 9% polarized orthogonal to this direction. These features give non-polar InGaN QDs unique advantages in polarization control over other materials, such as conventional polar nitride, InAs, or CdSe QDs. Hence, the ability to generate single photons with polarization control makes non-polar InGaN QDs highly attractive for quantum cryptography protocols.

Keywords: *a*-plane InGaN; deterministic polarization axis; **k·p** theory; linearly polarized single photon; quantum dots.

***Corresponding authors: Tong Wang,** Department of Physics, University of Oxford, Parks Road, Oxford OX1 3PU, UK, e-mail: tong.wang@physics.ox.ac.uk; and **Saroj K. Patra,** Tyndall National Institute, University College Cork, Cork, Ireland; Department of Electrical Engineering, University College Cork, Cork, Ireland, e-mail: sarojkanta.patra@tyndall.ie
Tim J. Puchtler and Robert A. Taylor: Department of Physics, University of Oxford, Parks Road, Oxford OX1 3PU, UK
Tongtong Zhu and Rachel A. Oliver: Department of Materials Science and Metallurgy, University of Cambridge, 27 Charles Babbage Road, Cambridge CB3 0FS, UK
Muhammad Ali and Tom J. Badcock: Cambridge Research Laboratory, Toshiba Research Europe Limited, 208 Science Park, Milton Road, Cambridge CB4 0FS, UK
Tao Ding: Department of Materials Science and Metallurgy, University of Cambridge, 27 Charles Babbage Road, Cambridge CB3 0FS, UK; and Nanophotonics Centre, Cavendish Laboratory, University of Cambridge, Cambridge CB3 0HE, UK
Stefan Schulz: Tyndall National Institute, University College Cork, Cork, Ireland

1 Introduction

Polarized single-photon sources [1, 2] are essential for applications in quantum information sciences, such as quantum key distribution [3–5] and optical quantum computing [6]. To develop these non-classical light sources, the nanophotonics of semiconductor quantum dots (QDs) [7–9] has been a field under intense scientific investigation. Although ultrapure and highly indistinguishable single-photon generation has been achieved in various arsenide-based QD systems [10–14], the large band offsets and strong exciton binding energies of III-nitride materials are needed for the realization of polarized photon emission [15–17] and room temperature operation [18, 19]. These polarized single-photon sources can then fulfill the need for on-chip polarization encoding in quantum cryptography, such as the BB84 protocol [20]. However, previous studies of polar *c*-plane (0001) InGaN QDs reveal that only selected QDs with large-shape anisotropies can exhibit high degrees of optical linear polarization (DOLP) [15, 16], which are also in agreement with our own investigations [21]. Furthermore, in most conventional *c*-plane nitride QD systems, different anisotropies could result in random polarization axes, which are highly undesirable in the implementation of polarization-based protocols in potential applications. Consequently, much effort is needed to define the anisotropy, in order to obtain consistently high DOLPs with deterministic polarization directions. Such experimental reports in the nitrides are limited to the manipulation of pyramidal geometries [22], elliptical QDs [23], or the use of nanowires [24, 25], where

the geometries of the structures make electrical contacting challenging. As such, a simpler and more practical method is needed to achieve polarization control, for the realization of on-chip polarized single-photon generation and related applications.

In this work, we report a combined theoretical and experimental investigation of a planar epitaxial self-assembled semiconductor QD system – non-polar *a*-plane (11–20) InGaN/GaN QDs – that provides not only a statistically high DOLP but also a fixed polarization direction determined by the underlying material crystallography. Furthermore, while the DOLPs of *a*-plane quantum wells (QWs) are limited to ~0.60 [26], we report a much higher average DOLP of ~0.90 in *a*-plane InGaN QDs. Previous investigations have reported polarization properties of some *a*-plane InGaN QDs along [0001] [27], orthogonal to those reported in *a*-plane QWs (along [1–100]) [26, 28, 29]. We find that this is a special case to the general behavior of *a*-plane QDs. Here, more rigorous measurements of the DOLP have been made upon a large number of QDs using high extraction efficiency QD-nanopillar structures. Theoretical simulations have also been undertaken to elucidate the origin of the linearly polarized emission, producing results in agreement with our experimental findings.

Furthermore, it is well known that for InGaAs/GaAs QD, shape anisotropies have a significant effect upon the optical polarization properties of the QDs [30]. The experimental observation of high DOLPs raises the question of how strongly shape anisotropies affect the optical properties of self-assembled *a*-plane InGaN/GaN QDs and, thus, how reliable these QDs might be in generating highly polarized photons. Hence, we also provide the first investigation of the effect of dot anisotropy on the DOLP of *a*-plane InGaN QDs, and couple our findings to insights from statistically significant experimental studies.

2 Materials and methods

2.1 MOCVD growth of the QD sample and fabrication of nanopillars

The *a*-plane InGaN QD sample was grown by metal-organic vapor phase epitaxy in a 6×2-in Thomas Swan close-coupled showerhead reactor on an *r*-plane sapphire substrate using trimethylgallium, trimethylindium, and ammonia as precursors. The *a*-plane GaN template was prepared using a silicon nitride (SiN_x) interlayer method to control the defect density [31]. After the deposition of a low temperature GaN nucleation layer at 500°C, a 1-µm-thick seed GaN layer was grown at 1050°C and a V/III ratio of 60. A single SiN_x interlayer was grown at 900°C using a silane (SiH_4) flow rate at 0.2 µmol min^{-1}. A three-dimensional growth step was carried out at a pressure of 300 Torr using a V/III ratio of 1900, which was followed by a two-dimensional coalescence step using a V/III ratio of 60 at 100 Torr. The as-grown *a*-plane GaN template, utilizing the SiN_x interlayer, has a dislocation density of 4×10^9 cm^{-2} and a basal plane stacking fault density of 2.6×10^5 cm^{-1} [31, 32].

The InGaN QDs were grown using a modified droplet epitaxy method [33]. A 2.5 nm thick InGaN epilayer was grown at 695°C and 300 Torr, which was immediately annealed in N_2 atmosphere for 30 s at the growth temperature. This annealing process results in the formation of In/Ga metallic droplets, which will re-react with ammonia during the GaN capping to form InGaN QDs (an initial ~10 nm GaN cap was grown at the InGaN growth conditions, and another ~15 nm GaN was grown at 1050°C using H_2 as the carrier gas). The QDs were positioned in the center of a 50-nm-thick intrinsic GaN layer (unintentionally doped GaN – uid GaN), which was clad by ~600 nm of Si-doped GaN (dopant concentration ~3×10^{18} cm^{-3}) at the bottom and ~200 nm of Mg doped GaN (dopant concentration ~3×10^{19} cm^{-3}) on the top. An atomic force microscopy (AFM) image of an uncapped sample following the growth and anneal of the InGaN layer and a schematic of the full sample structure are shown in Figure 1A and B, respectively.

Silica nanospheres (d≈180 nm, fabricated in our laboratory [34]) were dispersed in ethanol and deposited onto the sample by drop casting. The nanospheres act as the etch mask for the nanopillars. The sample was subsequently dry-etched in an Oxford Instruments PlasmaPro 100 inductively coupled plasma etch system to a depth of ~350 nm using a gas mixture of Cl_2 and Ar. The residual silica nanospheres were removed by ultra-sonication in acetone, followed by a buffered oxide etch. SEM images of the nanopillars before and after the removal of the residual silica nanospheres are shown in Figure 1C and D, respectively, where the diameter at the top of the nanopillar is ~180 nm. The tapered shape is formed naturally during the dry-etching process.

2.2 Optical characterization

The sample was mounted in an AttoDRY800 closed-cycle cryogenic system that maintains a stable sample temperature of 5 K. As shown in Figure 1E, an 80-MHz Ti:Sapphire laser system generates 1-ps pulses at 800 nm, providing

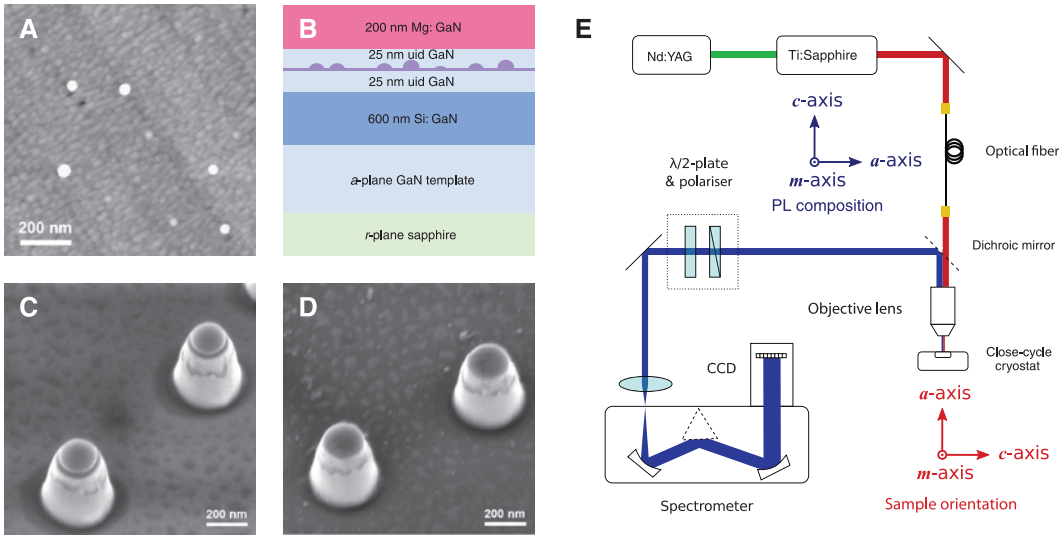

Figure 1: Sample structure, processing, and setup of optical experiment.
(A) AFM image of an uncapped QD sample grown on *a*-plane GaN template, with *z*-scale = 5 nm. (B) Schematic material structure for the nanopillar p-i-n sample with InGaN QDs. Also shown are SEM images (30° tilted view) of nanopillars (C) before and (D) after the removal of the residual silica nanospheres. (E) Schematic of polarization-resolved micro-photoluminescence (μ-PL) setup, illustrating the sample orientation and consequent PL composition before passing through the polarizer in the plane of view.

two-photon excitation for the sample. It has been previously established that under multiphoton excitation, structures with higher degrees of quantum confinement have greater relative absorption cross-section [35]. As such, a two-photon excitation produces better signal-to-background ratios for our sample, which contains both QDs and a fragmented QW.

A single-mode fiber with a 4-μm core spatially filters and transmits the excitation laser pulses onto a collimating lens, which then passes the beam to a 100× NIR objective with a numerical aperture of 0.5, producing an ~1-μm laser spot for sample excitation. A power density of 2 MW cm^{-2} is chosen so that the QDs have the strongest emission before saturation takes place. Because of the use of two-photon excitation, this power is higher than the typical ~kW cm^{-2} intensity used in one-photon excitation. The PL from the sample is then collected by the same objective and directed to an Andor Shamrock 500i half-meter spectrograph with variable slit size and a grating of 1200 lines mm^{-1}. An AndoriDus 420 Si-based charge-coupled device (CCD) is thermoelectrically cooled to –50°C for low-noise detection, enabling μ-PL measurements with a spectral resolution of ~38 pm. The PL can also be spectrally filtered and passed on to a pair of photomultiplier tubes for standard Hanbury Brown and Twiss measurements.

For polarization-resolved μ-PL, a rotatable polarizer cube and a half-wave plate are introduced in the optical collection path. The transmission axis of the polarizer is set to 0° on the rotation mount and aligned parallel to the *c*-axis component of the sample PL. Hence, a polarizer rotation of θ would correspond to the angle away from the *c*-axis in the growth plane, as shown in Figure 1E.

Ensuring high accuracy in polarization-resolved μ-PL spectroscopy is experimentally challenging in a number of ways, including random sample drift, PL intensity fluctuations, and difficulty in measurement when approaching the weaker polarized component. In order to ensure the precision of measurement as far as possible, three precautions have been taken during the course of measurement: (1) The half-wave plate was rotated by $-\theta/2$ for a polarizer angle of θ, thus, maintaining a constant axis of PL polarization and correcting an ~10% difference in polarization-sensitive detection of the system. (2) The slit of the spectrometer was opened wide enough to account for slight optical alignment changes caused by the rotation of the polarizer cube, so that PL intensity remained constant at angles 180° apart. (3) To counteract any sample position drift, a reference measurement of the maximum intensity was immediately made after the data at each θ was taken, and μ-PL results were normalized accordingly during analysis.

2.3 Theoretical simulations

To address the electronic and optical properties of *a*-polar InGaN/GaN QDs from a theoretical perspective, we applied a flexible **k·p** model, accounting for strain and

built-in fields, as described in detail elsewhere [17, 36–38]. To study the DOLP, band mixing effects in the valence band are of central importance. As such, a six-band Hamiltonian to describe the hole states and a single-band effective mass approximation for electrons are used. In the following study, the *x*-axis of our coordinate system is parallel to the crystal *c*-axis. A schematic illustration of the coordinate system is given in the inset of Figure 2A.

3 Results and discussion

3.1 Theoretical calculations of DOLP

Information regarding the QD geometry and indium content, which is difficult to obtain experimentally, is required for calculation inputs. Previous studies on InGaN QD systems assumed lens-shaped geometries [39, 40]. We followed this assumption, and based on earlier AFM results [33], chose a base diameter of 30 nm and a height of 2.5 nm as our starting point, with indium content varied between 15% and 25%. All calculations were performed on a $50\times50\times30$-nm^3 supercell with periodic boundary conditions. With these assumptions, the calculated ground state transition energies were in the range of 2.7 to 2.9 eV, close to typical experimental values [27, 32, 33, 41–44] and those discussed below. Therefore, the chosen geometries and indium contents should give a reasonable description of the structures considered here. A detailed analysis of built-in fields, electronic structure, excitonic and biexcitonic properties of the systems under consideration is given in Ref. [36].

The outcome of our **k·p** calculations for a dot with a circular base predicted a hole ground state with 97% $|Y\rangle$-like and only 2% $|X\rangle$- like character, indicating that the emitted light should be polarized perpendicular to the *c*-axis (along the *m*-axis). The intensities measured perpendicular and parallel to the wurtzite *c*-axis, $I_\perp$ and $I_\parallel$, should reflect largely the $|Y\rangle$- and $|X\rangle$- like orbital contributions to the hole ground state, respectively. According to the DOLP formula, $\rho=(I_\perp-I_\parallel)/(I_\perp+I_\parallel)$, an *a*-plane InGaN QD with a circular base is, hence, predicted to have a ρ of 0.96. This result is in stark contrast with theoretical studies of *c*-plane InGaN QDs, where ρ, due to the *c*-plane symmetry, is 0 for dots with no in-plane anisotropies [15, 16].

However, it is important to note that self-assembled QDs are unlikely to be perfectly symmetrical. Results on both InGaAs QDs [30] and *c*-plane InGaN QDs [15, 16] reveal that dot shape anisotropy plays an important role and affects their properties quite significantly due to band mixing effects. Anisotropy affects the degree of quantum confinement, which causes energetic shifts in the $|X\rangle$-, $|Y\rangle$- and $|Z\rangle$-like state and, thus, their contribution to the band mixing effects for the hole ground state. It is, therefore, important to study how significant this effect is in our QDs by modifying the dot geometry in the simulation. We define the in-plane aspect ratio α as $\alpha=d_x/d_y$, where d_x and d_y are the in-plane dimensions of the dot base along the *x*- and *y*-directions, respectively. Here, for a circular base, $d_x=d_y=30$ nm, and $\alpha=1$. A schematic illustration of the convention is given in the inset of Figure 2A.

A smaller dimension, and thus stronger confinement effects, along the *x*-direction will further increase the

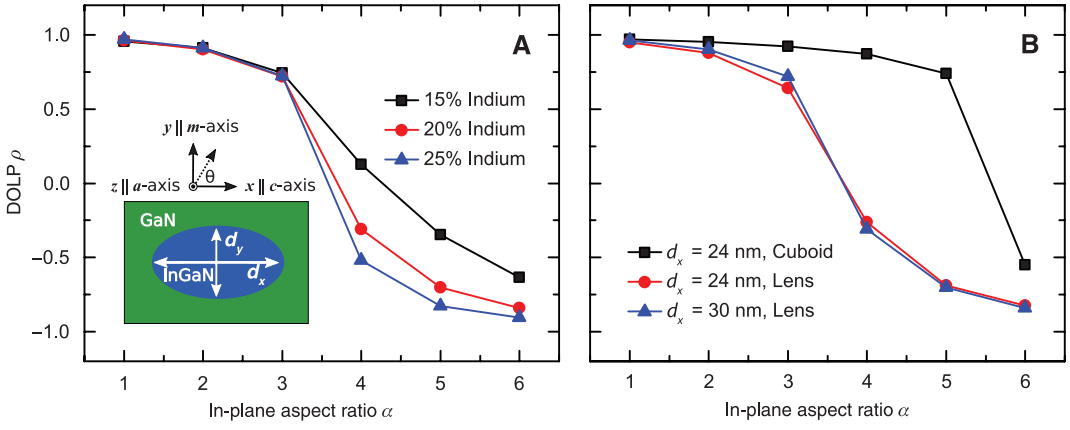

Figure 2: (A) DOLP ρ as a function of the in-plane aspect ratio α and indium content of a lens-shaped *a*-plane InGaN/GaN QD. The inset shows the coordinate system, the definition of θ as the in-plane angle away from the crystal *c*-axis (same as that defined in the experimental setup), and the definitions of d_y and d_x as the in-plane dimensions of a QD used in the theoretical investigation. α is defined as $\alpha=d_x/d_y$. (B) ρ as a function of α, size, and geometry of a QD.

DOLP as it approaches unity. This is attributed to the lower effective mass of the $|X\rangle$-like states along this direction and an increase in the energetic separation of $|Y\rangle$- and $|X\rangle$-like states. Correspondingly, the more interesting situation is what happens if the dot geometry is modified along the y-direction. Such an anisotropy should affect states with a high $|Y\rangle$-like orbital contribution more strongly, again due to the fact that $|Y\rangle$-like ($|X\rangle$-like) states exhibit a low (high) effective mass along the y-direction [45]. Please note that the coordinate system used in this work is different from that used in Ref. [45]. More details on the coordinate system used here can be found in Ref. [38]. Hence, calculations were performed at $d_y = 30$, 15, 7, 6, and 5 nm, as the QD base becomes more elliptical. The results for ρ as a function of α and indium content are shown in Figure 2A. We see that ρ is almost constant for α values between 1 and 2, and decreases only slightly for $\alpha = 3$, independent of indium content. It is important to note that $\alpha = 3$ already presents a significant "deformation" of the dot ($d_x = 30$, $d_y = 10$). Consequently, the calculations show that in a-plane InGaN QDs, the DOLP ρ is very insensitive against shape anisotropies and indium composition changes. It should be noted that, in principle, Coulomb effects can mix contributions from excited (single-particle) states into the excitonic ground state [46]. However, our calculations reveal that the first few excited hole states are all almost entirely $|Y\rangle$-like in character. Thus, mixing of different hole states via Coulomb effects will not affect the orbital character discussed here. A detailed discussion of excited states and how this affects the DOLP at elevated temperatures is beyond the scope of the present study and will be reported elsewhere.

To strengthen the argument that the DOLP is extremely robust against shape anisotropies, we have also varied the geometry and size of the dot. First, to study the impact of the QD size on the DOLP, we have kept the geometry to be lens-shaped but reduced the in-plane dimensions of the system. Here, for the symmetric dot, $d_x = d_y = 24$ nm. To consider the same range of in-plane aspect ratios α, d_y has been varied between 24 and 4 nm. The results of this study are shown in Figure 2B (red circles), revealing that the change in the QD in-plane dimensions affects the DOLP only very slightly.

To further extend this analysis, we have also investigated the influence of the QD geometry on the DOLP. To this end, we have drastically changed the QD geometry from a lens-shaped dot to a cuboid. The length and width of the cuboid is assumed to be of 24 nm with a height of 2.5 nm. Figure 2B shows the data (black squares) of the DOLP as a function of α for the cuboidal dot. As one can infer from this study, in comparison with the lens-shaped systems, the reduction of the DOLP only happens at higher α values ($\alpha = 5$). Consequently, the DOLP in cuboid-shaped dots would even be more robust against shape anisotropies.

As such, our theoretical studies predict high experimental DOLP values, with very small variations caused by QD shape anisotropies, indium content variations, size, and geometry differences. To validate the simulation results and gain further insights from the experiments, we perform optical characterization of non-polar a-plane InGaN/GaN QDs.

3.2 Experimental and statistical investigations of QD emission

The PL spectra of the two cross-polarized components of a single QD are shown in Figure 3, with its emission intensities at 10° intervals displayed in the right inset. The data were fitted with $I(\theta) = I_{\perp}\cos^2(\theta-\varphi) + I_{\parallel}\sin^2(\theta-\varphi)$, where $I_{\perp}$, $I_{\parallel}$, and θ follow the same definitions explained previously, and φ is the angle at which the maximum of function

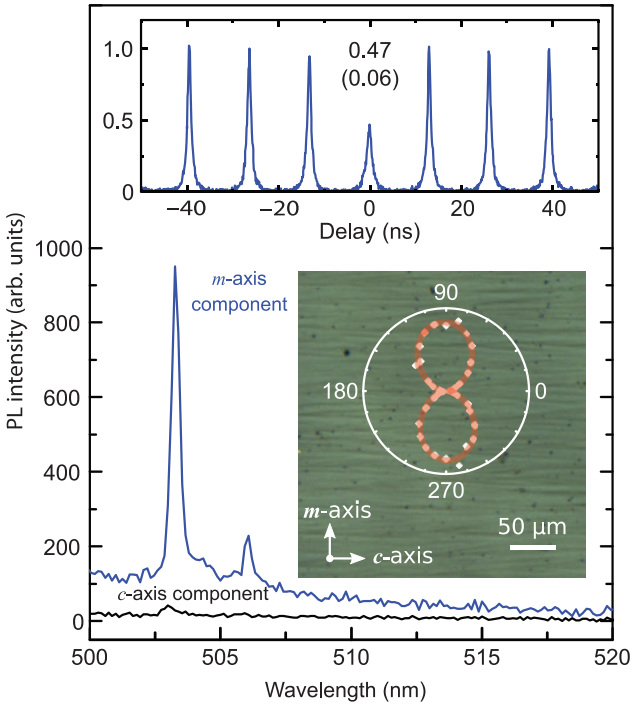

Figure 3: The μ-PL of the two cross-polarized components for a QD at 503 nm (~2.46 eV). Top inset demonstrates the emission of single photons with a raw $g^{(2)}(0)$ of 0.47, which becomes 0.06 after a standard background correction (~75% QD intensity). Right inset shows sinusoidal intensity variation of the QD emission and axis of polarization with respect to striations on the sample surface.

occurs. As both cross-polarized components should exhibit Malus' law type intensity variation, two sinusoidal fits with a phase difference of 90° are used in the equation. The sinusoidal intensity change, thus, demonstrates that the QD emission is polarized. Furthermore, the φ is found to be $92° \pm 1°$, indicating that the maximum intensity occurs at $\theta = 92°$ and 272°, indeed corresponding to the direction perpendicular to the *c*-axis. The small difference of ~2° is attributed to the error of sample placement in the cryostat.

According to the illustration in Figure 1E and the definition of θ, the polarization axis can, hence, be determined to be along the *m*-axis, the same as the simulation predicts. To further quantify how polarized the emission is, we invoked the DOLP formula described previously and calculated a ρ of 0.92 for this QD, again showing good agreement with the theoretical results for α values between 1 and 2.

Additionally, the intensity variation plot is shown on top of an optical microscope image of the sample. The *a*-plane sample surface exhibits striated features along the *c*-axis [31], further demonstrating the orthogonality between the polarization axis and the crystal *c*-direction. As such, the PL polarized parallel to the *c*-axis should correspond to the weaker polarized component of QD emission, instead of the stronger one as previously reported [27].

In order to achieve statistical significance for this finding, we investigated the absolute values of DOLP of 180 QDs individually. In this investigation, only QDs with a peak intensity of >50 counts s^{-1} were included in this investigation, in order to ensure measurement accuracy. The distribution of $|\rho|$ for these QDs is shown in Figure 4A. The high mean $|\rho|$ of 0.90 provides direct evidence that non-polar *a*-plane InGaN QDs are strongly polarized photon emitters. Furthermore, due to the modified droplet epitaxy growth routine [33], the *a*-plane QDs studied in this work were formed on top of fragmented QWs (fQWs). In the μ-PL experiments, we observe sharp emission features from the QDs together with the underlying fQW emission over the same spectral range, such as that in Figure 3. As such, we are able to not only measure the DOLP for the QDs but also for the underlying *a*-plane fQWs. For each of the 180 *a*-plane QDs we investigated, the $|\rho|$ of their respective fQWs are shown in Figure 4B.

All $|\rho|$ data of QDs fall in the range between 0.60 to 1.00, in contrast to those of QWs between 0 and 0.80. The average $|\rho|$ of 0.46 for the QWs, which is in agreement with the latest literature findings [26], is also much less than the average of 0.90 for the QDs. From a fundamental perspective, this is interesting because out of *a*-plane nanostructures, only *a*-plane QDs possess such high DOLPs. From a technology viewpoint, coupled with the ability to achieve single-photon emission, *a*-plane QDs are well suited for the generation of single photons with polarization control and useful for the development of quantum information applications. A typical $g^{(2)}(0)$ measurement from one of our dots is shown in the top inset in Figure 3, where we measure emission of single photons with a raw $g^{(2)}(0)$ of 0.47, which becomes 0.06 after a standard background correction (~75% QD intensity).

The spread of the values in Figure 4A is attributed to variations of QD size, shape, and indium content. There are 23 QDs for which the weaker polarized component cannot be detected at all, giving a DOLP of unity. As explained in the theoretical simulation, this could be caused by a compression of the QD geometry along the

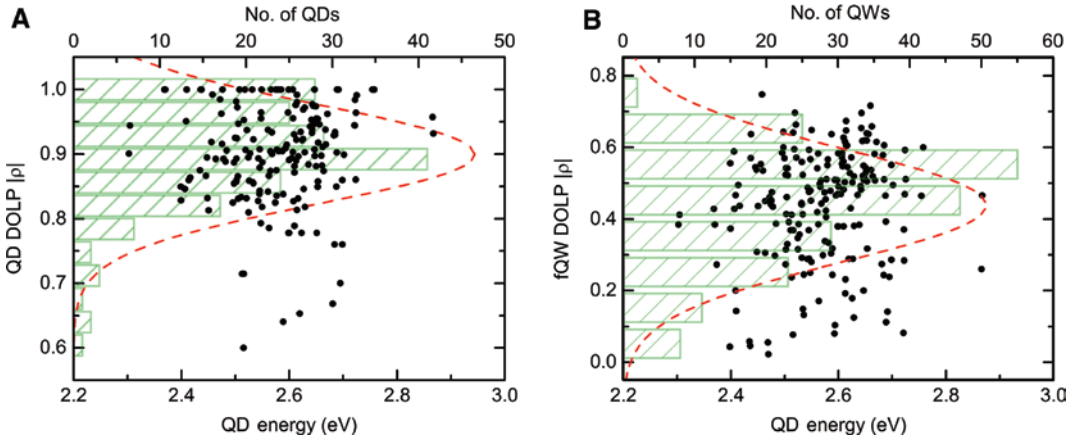

Figure 4: The 180 *a*-plane InGaN/GaN (A) QD and (B) underlying QW DOLP variation with emission energy.
The statistical distributions have been fitted with Gaussian profiles. The means and standard deviations of the Gaussian distributions are (A) 0.90 ± 0.08 and (B) 0.46 ± 0.14, respectively.

c-direction. Those with DOLP values lower than average could be attributed to a compression along the *m*-axis (cf. Figure 2A and B). Furthermore, the calculated standard deviation is only 0.08, which signifies very small fluctuations around the high average DOLP. As such, the robustness of DOLP against changes in size, shape anisotropy, and indium content have been demonstrated both theoretically and experimentally. The data in Figure 4A and B indicate that there are no discernible correlations between QD energy and DOLP (of their respective QW), thus, *a*-plane InGaN QDs emit highly polarized photons across all attainable wavelengths.

The alignment of the polarization axis was also studied during the polarization measurement. In order to avoid selection bias, the polarizer was initially set to 45°. For each QD emission observed in the PL spectrum, the polarizer was then rotated from 0° to 90°, to determine the angle at which the maximum and minimum intensities occurred. Of the QDs, 91% exhibit polarization aligned along the *m*-axis (within a 10° error), which agrees with the simulation results. However, there are 9% of the studied QDs polarized along the *c*-axis. In our theoretical framework, this would mean that the hole ground state is predominantly $|X\rangle$-like in orbital character. From Figure 2A, one can infer that ρ drops significantly for $\alpha > 3$, and more so with higher indium content, as the confinement effects due to increased band offsets become stronger, making asymmetries in the QD geometry more prominent. Producing a predominant $|X\rangle$-like hole ground state would, hence, require an extreme deformation of the QD ($d_x = 30$ nm, $d_y = 6$ nm) and very high indium content. In addition to strong shape anisotropies, alloy fluctuation effects might also contribute to the observed behavior [47]. As such, the previous report [27] is an investigation of these 9% QDs, which is a special case to the general behavior of *a*-plane InGaN QDs. It is also worth noting that the DOLPs of such QDs are similarly high and follow the same distribution as that shown in Figure 4A.

An example of an *a*-plane QD polarized along the *c*-direction, as one of the 9% cases, is shown in Figure 5. The QD at ~505 nm has its maximum intensity at $\theta = 0°$, corresponding to a polarization axis along the crystal *c*-direction. However, the underlying *a*-plane fQW still behaves as expected, and has its maximum intensity at $\theta = 90°$. The QD has a DOLP of unity, and the QW has a DOLP of 0.27, both of which are in agreement with the statistics in Figure 4A and B, respectively. As such, we show evidence of cross-polarized QD and QW emissions from our *a*-plane InGaN QD sample. Because of the suppression of the QW background in these 9% cases, we are able

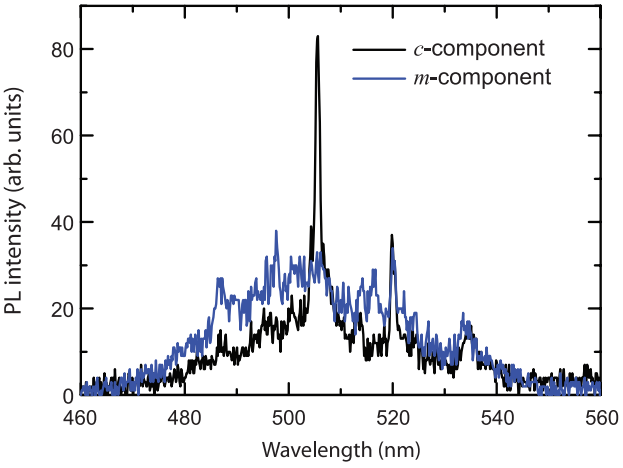

Figure 5: The μ-PL of a QD (~505 nm) and its underlying fQW. The QD is polarized along the *c*-direction, while the fQW is polarized along the *m*-direction, corresponding to one of the 9% special cases in which *a*-plane QDs are polarized parallel to the crystal *c*-axis.

to achieve higher dot-to-background ratios for the QDs with a polarization axis along the *c*-axis, which are beneficial for the development of purer single-photon sources than that shown in Figure 3, with $g^{(2)}(0)$ values closer to 0. Overall, our experimental and theoretical data show that compared to QDs fabricated with *c*-plane nitrides, arsenides, or other semiconductor materials, *a*-plane InGaN/GaN QDs are able to achieve efficient linearly polarized single-photon emission with consistently high DOLPs and a deterministic polarization axis.

4 Conclusions

In conclusion, this work provides a statistically significant investigation of the polarization properties of *a*-plane InGaN QDs with high experimental precision. Cross-polarized photon emissions from 180 QDs produce an average DOLP as high as 0.90, with a small standard deviation of only 0.08. Theoretical **k·p** simulations have also demonstrated similarly high DOLP for these QDs, which is almost insensitive to small size differences, shape anisotropies, and indium content changes. The polarization axis has been theoretically and experimentally determined to be mostly along the crystallographic *m*-axis direction, with a small (9%) minority along the *c*-axis. It is also important to note that the studied *a*-plane InGaN QD systems outperform *a*-plane QW systems in terms of the DOLP. The statistically high DOLP, fixed polarization axis, and insensitivity to size, shape, and indium contents offer *a*-plane InGaN QDs unique advantages in polarization

control compared to their *c*-plane InGaN and GaN counterparts, and to QDs based on other materials, such as InAs or CdSe. In summary, polarized single-photon sources based on the non-polar *a*-plane InGaN QD system are good candidates for the development of quantum information applications.

Acknowledgments: This research was supported by the UK Engineering and Physical Sciences Research Council (EPSRC) Grants EP/M012379/1 and EP/M011682/1, and the Science Foundation Ireland (Project No. 13/SIRG/2210). T.W. is also grateful for the award of the National Science Scholarship (NSS) as PhD funding by the Singapore Agency for Science, Technology and Research (A*STAR).

References

[1] Aharonovich I, Englund D, Toth M. Solid-state single-photon emitters. Nat Photonics 2016;10:631–41.
[2] Lounis B, Orrit M. Single-photon sources. Reports Prog Phys 2005;68:1129–79.
[3] Muller A, Breguet J, Gisin N. Experimental demonstration of quantum cryptography using polarized photons in optical fiber over more than 1 km. Eur Lett 1993;23:383–8.
[4] Kurtsiefer C, Zarda P, Halder M, et al. Quantum cryptography:a step towards global key distribution. Nature 2002;419:450.
[5] Peng CZ, Yang T, Bao XH, et al. Experimental free-space distribution of entangled photon pairs over 13 km:towards satellite-based global quantum communication. Phys Rev Lett 2005;94:150501.
[6] Loss D, DiVincenzo DP. Quantum computation with quantum dots. Phys Rev A 1998;57:120–6.
[7] Santori C, Pelton M, Solomon G, Dale Y, Yamamoto Y. Triggered single photons from a quantum dot. Phys Rev Lett 2001;86:1502–5.
[8] Buckley S, Rivoire K, Vučković J. Engineered quantum dot single-photon sources. Reports Prog Phys 2012;75:126503.
[9] Michler P, Kiraz A, Becher C, et al. A quantum dot single-photon turnstile device. Science 2000;290:2282–5.
[10] Gschrey M, Thoma A, Schnauber P, et al. Highly indistinguishable photons from deterministic quantum-dot microlenses utilizing three-dimensional in situ electron-beam lithography. Nat Commun 2015;6:7662.
[11] He Y-M, He Y, Wei Y-J, et al. On-demand semiconductor single-photon source with near-unity indistinguishability. Nat Nanotechnol 2013;8:213–7.
[12] Somaschi N, Giesz V, De Santis L, et al. Near-optimal single-photon sources in the solid state. Nat Photonics 2016;10:340–5.
[13] Wei Y, He Y-M, Chen M, et al. Deterministic and robust generation of single photons on a chip with 99.5% indistinguishability using rapid adiabatic passage. Nano Lett 2014;14:6515.
[14] Ding X, He Y, Duan ZC, et al. On-demand single photons with high extraction efficiency and near-unity indistinguishability from a resonantly driven quantum dot in a micropillar. Phys Rev Lett 2016;116:020401.
[15] Bardoux R, Guillet T, Gil B, et al. Polarized emission from GaN/AlN quantum dots:single-dot spectroscopy and symmetry-based theory. Phys Rev B 2008;77:235315.
[16] Jemsson T, Machhadani H, Holtz PO, Karlsson KF. Polarized single photon emission and photon bunching from an InGaN quantum dot on a GaN micropyramid. Nanotechnology 2015;26:065702.
[17] Patra SK, Marquardt O, Schulz S. Polar, semi- and non-polar nitride-based quantum dots:influence of substrate orientation and material parameter sets on electronic and optical properties. Opt Quantum Electron 2016;48:151.
[18] Holmes MJ, Kako S, Choi K, Arita M, Arakawa Y. Single photons from a hot solid-state emitter at 350 K. ACS Photonics 2016;3:543–6.
[19] Deshpande S, Frost T, Hazari A, Bhattacharya P. Electrically pumped single-photon emission at room temperature from a single InGaN/GaN quantum dot. Appl Phys Lett 2014;105:141109.
[20] Bennett CH, Brassard G. Quantum cryptography: public key distribution and coin tossing. Proceedings of IEEE International Conference on Computers, Systems, and Signal Processing 1984:175–9.
[21] Reid BPL. Towards cavity quantum electrodynamics and coherent control with single InGaN/GaN quantum dots. PhD Thesis (University Oxford) 2013:52–5.
[22] Lundskog A, Hsu C-W, Fredrik Karlsson K, et al. Direct generation of linearly polarized photon emission with designated orientations from site-controlled InGaN quantum dots. Light Sci Appl 2014;3:e139.
[23] Teng C-H, Zhang L, Hill T, Demory B, Deng H, Ku P-C. Elliptical quantum dots as on-demand single photons sources with deterministic polarization states. Appl Phys Lett 2015;107:191105.
[24] Deshpande S, Heo J, Das A, Bhattacharya P. Electrically driven polarized single-photon emission from an InGaN quantum dot in a GaN nanowire. Nat Commun 2013;4:1675.
[25] Puchtler TJ, Wang T, Ren CX, et al. Ultrafast, polarized, single-photon emission from m-plane InGaN quantum dots on GaN nanowires. Nano Lett 2016;16:7779–85.
[26] Kundys D, Sutherland D, Davies MJ, et al. A study of the optical and polarisation properties of InGaN/GaN multiple quantum wells grown on a-plane and m-plane GaN substrates. Sci Technol Adv Mater 2016;17:736–43.
[27] Reid BPL, Kocher C, Zhu T, et al. Non-polar InGaN quantum dot emission with crystal-axis oriented linear polarization. Appl Phys Lett 2015;106:171108.
[28] Badcock TJ, Dawson P, Kappers MJ, et al. Optical polarization anisotropy of a-plane GaN/AlGaN multiple quantum well structures grown on r-plane sapphire substrates. J Appl Phys 2009;105:123112.
[29] Chiu CH, Kuo SY, Lo MH, et al. Optical properties of a-plane InGaN/GaN multiple quantum wells on r-plane sapphire substrates with different indium compositions. J Appl Phys 2009;105:063105.
[30] Schliwa A, Winkelnkemper M, Bimberg D. Impact of size, shape, and composition on piezoelectric effects and electronic properties of In(Ga)As⁄GaAs quantum dots. Phys Rev B 2007;76:205324.
[31] Oehler F, Sutherland D, Zhu T, et al. Evaluation of growth methods for the heteroepitaxy of non-polar (11–20) GAN on sapphire by MOVPE. J Cryst Growth 2014;408:32–41.

[32] Emery RM, Zhu T, Oehler F, et al. Non-polar (11–20) InGaN quantum dots with short exciton lifetimes grown by metal-organic vapour phase epitaxy. Phys Status Solidi C 2014;11:698–701.
[33] Zhu T, Oehler F, Reid BPL, et al. Non-polar (11–20) InGaN quantum dots with short exciton lifetimes grown by metalorganic vapor phase epitaxy. Appl Phys Lett 2013;102:251905.
[34] Liu ZF, Ding T, Zhang G, Song K, Clays K, Tung CH. Ternary inverse opal system for convenient and reversible photonic bandgap tuning. Langmuir 2008;24:10519–23.
[35] Jarjour AF, Green AM, Parker TJ, et al. Two-photon absorption from single InGaN/GaN quantum dots. Physica E 2006;32:119–22.
[36] Patra SK, Schulz S. Non-polar $In_xGa_{1-x}N$/GaN quantum dots:impact of dot size and shape anisotropies on excitonic and biexcitonic properties. J Phys D Appl Phys 2017;50:025108.
[37] Marquardt O, Boeck S, Freysoldt C, et al. A generalized plane-wave formulation of **k·p** formalism and continuum-elasticity approach to elastic and electronic properties of semiconductor nanostructures. Comput Mater Sci 2014;95:280–7.
[38] Schulz S, Marquardt O. Electronic structure of polar and semi-polar (11-22)-oriented nitride dot-in-a-well systems. Phys Rev Appl 2015;3:064020.
[39] Schuh K, Barthel S, Marquardt O, et al. Strong dipole coupling in nonpolar nitride quantum dots due to Coulomb effects. Appl Phys Lett 2012;100:092103.
[40] Barthel S, Schuh K, Marquardt O, et al. Interplay between Coulomb interaction and quantum-confined Stark-effect in polar and nonpolar wurtzite InN/GaN quantum dots. Eur Phys J B 2013;86:449.
[41] Reid BPL, Zhu T, Chan CCS, et al. High temperature stability in non-polar (11–20) InGaN quantum dots:exciton and biexciton dynamics. Phys Status Solidi C 2014;11:702–5.
[42] Reid BPL, Kocher C, Zhu T, et al. Observations of Rabi oscillations in a non-polar InGaN quantum dot. Appl Phys Lett 2014;104:263108.
[43] Reid BPL, Zhu T, Puchtler TJ, et al. Origins of spectral diffusion in the micro-photoluminescence of single InGaN quantum dots origins of spectral diffusion in the micro-photoluminescence of single InGaN quantum dots. Jpn J Appl Phys 2013;52:08JE01.
[44] Griffiths JT, Zhu T, Oehler F, et al. Growth of non-polar (11–20) InGaN quantum dots by metal organic vapour phase epitaxy using a two temperature method. APL Mater 2014;2:126101.
[45] Schulz S, Badcock TJ, Moram MA, et al. Electronic and optical properties of nonpolar a-plane GaN quantum wells. Phys Rev B 2010;82:125318.
[46] Baer N, Schulz S, Gartner P, Schumacher S, Czycholl G, Jahnke F. Influence of symmetry and Coulomb correlation effects on the optical properties of nitride quantum dots. Phys Rev B 2007;76:075310.
[47] Schulz S, Tanner DP, O'Reilly EP, et al. 2015 Structural, electronic, and optical properties of m-plane InGaN/GaN quantum wells:insights from experiment and atomistic theory. Phys Rev B 2015;92:235419.

Article note: All data presented in Figures 2–5 are available free of charge at the DOI: 10.5287/bodleian:4RKDBkoVe.